

Bayesian model comparison in cosmology with Population Monte Carlo

Martin Kilbinger^{1,2*}, Darren Wraith^{3,1}, Christian P. Robert³, Karim Benabed¹, Olivier Cappé⁴, Jean-François Cardoso^{4,1}, Gersende Fort⁴, Simon Prunet¹, François R. Bouchet¹

¹ *Institut d’Astrophysique de Paris, UMR 7095 CNRS & Université Pierre et Marie Curie, 98 bis boulevard Arago, 75014 Paris, France*

² *Shanghai Key Lab for Astrophysics, Shanghai Normal University, Shanghai 200234, P. R. China*

³ *CEREMADE, Université Paris Dauphine, 75016 Paris, France*

⁴ *LTCI, Telecom ParisTech and CNRS, 46, rue Barrault, 75013 Paris, France*

4 July 2021

ABSTRACT

We use Bayesian model selection techniques to test extensions of the standard flat Λ CDM paradigm. Dark-energy and curvature scenarios, and primordial perturbation models are considered. To that end, we calculate the Bayesian evidence in favour of each model using Population Monte Carlo (PMC), a new adaptive sampling technique which was recently applied in a cosmological context. In contrast to the case of other sampling-based inference techniques such as Markov chain Monte Carlo (MCMC), the Bayesian evidence is immediately available from the PMC sample used for parameter estimation without further computational effort, and it comes with an associated error evaluation. Besides, it provides an unbiased estimator of the evidence after any fixed number of iterations and it is naturally parallelizable, in contrast with MCMC and nested sampling methods. By comparison with analytical predictions for simulated data, we show that our results obtained with PMC are reliable and robust. The variability in the evidence evaluation and the stability for various cases are estimated both from simulations and from data. For the cases we consider, the log-evidence is calculated with a precision of better than 0.08.

Using a combined set of recent CMB, SNIa and BAO data, we find inconclusive evidence between flat Λ CDM and simple dark-energy models. A curved Universe is moderately to strongly disfavoured with respect to a flat cosmology. Using physically well-motivated priors within the slow-roll approximation of inflation, we find a weak preference for a running spectral index. A Harrison-Zel’dovich spectrum is weakly disfavoured. With the current data, tensor modes are not detected; the large prior volume on the tensor-to-scalar ratio r results in moderate evidence in favour of $r = 0$.

Key words: cosmological parameters – methods: statistical

1 INTRODUCTION

We have reached an era of precision cosmology, as impressive constraints on cosmological parameters attest (e.g. Dunkley et al. 2009, among many others). Parameters of the standard Λ CDM model are measured with uncertainties of a few percent. At the same time, we have not made the transition to

what Peebles (2002) called ‘accurate cosmology’. This next and qualitatively different step involves the scrutiny of the underlying model rather than the ever more precise determination of model parameters. This approach is particularly important in the field of cosmology which relies on a considerable extrapolation of known physics to large scales and high energies (in the early Universe), and lacks physical understanding, e.g. of the dark sector. Subsequently, cosmology has spawned a multitude of different models.

* E-mail: kilbinger@iap.fr

There are several statistical approaches for comparing competing models. Most of them aim at a balance between the ability of a model to fit observational data, and its complexity. While information theory approaches like Akaike's criterion (AIC, Akaike 1974) provide explicit penalisations for the complexity of a model, Bayesian analysis compares directly the posterior probabilities of models, in favour of each of one of the given models. In that sense, Bayesian analysis has often been argued to propose an automated Occam's razor, see e.g. Berger & Jeffreys (1992), or MacKay (2002). Following the classical Bayesian approach (Jeffreys 1939), the comparison between models integrates out the parameters within each model and automatically penalises larger parameter spaces.

From a practical viewpoint, especially for high-dimensional parameter spaces, the calculation of the evidence is very challenging. While fast approximations exist, such as BIC (Schwarz 1978), Laplace (see e.g. Heavens et al. 2007), or variational Bayes (e.g. MacKay 2002), they can fail dramatically for posterior distributions which are not well approximated by a multivariate Gaussian.

Recently, a new adaptive importance sampling method called Population Monte Carlo (PMC) was introduced (Cappé et al. 2004, 2008) and successfully tested in a cosmological context (Wraith et al. 2009, hereafter WKB09). PMC has since been used for a range of applications in cosmology (Benabed et al. 2009; Ménard et al. 2009; Schrabback et al. 2009).

WKB09 focused on parameter estimation with the PMC sampling algorithm. In this second paper, we use the PMC method to estimate the Bayesian evidence and assess the accuracy and reliability of this estimate. We emphasize that the same set of sampled values used for parameter estimation can also be used to calculate the Bayesian evidence. Thus with the PMC method, model selection comes at the same computational cost as parameter estimation.

This paper is organised as follows: We describe the basics of the PMC algorithm in Sect. 2. Section 3 assesses the performance and reliability of PMC to calculate the Bayesian evidence using numerical simulations. In Sect. 4 we use PMC to compare cosmological models in the context of dark energy and primordial perturbations. Our findings are summarised in Sect. 5.

2 BAYESIAN MODEL SELECTION WITH POPULATION MONTE CARLO

2.1 Bayesian evidence and Bayes' factor

The Bayesian evidence E in favour of a model \mathfrak{M} with likelihood function L and prior distribution P is the average of the likelihood function over the parameter space

$$E = \int L(x)P(x) dx = \int \pi(x) dx, \quad (1)$$

where $\pi(x) = L(x)P(x)$ is the unnormalised posterior. We denote the normalised posterior density by $\bar{\pi}(x)$, the normalisation constant being the evidence, $\bar{\pi}(x) = \pi(x)/E$.

The Bayes factor (Jeffreys 1939) is the ratio of the evidences E_1 and E_2 for two competing models \mathfrak{M}_1 and \mathfrak{M}_2 ,

Table 1. Jeffrey's scale to quantify the 'strength of evidence' for a corresponding range of the Bayes factor B_{12} in (2), assuming $B_{12} > 1$.

$\ln B_{12}$	B_{12}	Strength
< 1	< 2.7	Inconclusive
$1 \dots 2.5$	$2.7 \dots 12$	Weak
$2.5 \dots 5$	$12 \dots 150$	Moderate
> 5	> 150	Strong

respectively,

$$B_{12} = \frac{E_1}{E_2}. \quad (2)$$

If B_{12} is larger (smaller) than unity, the data favour model \mathfrak{M}_1 (\mathfrak{M}_2) over the alternative model. To quantify the 'strength of evidence' contained in the data, Jeffreys (1961) introduced an empirical scale, see Table 1. This is only a rough guideline for decision making and of course the proposed boundaries are mostly subjective. For a comprehensive review of Bayesian model selection, we refer the interested reader to Chen et al. (2000) and Trotta (2008).

2.2 A note on priors

The Bayesian evidence depends crucially on the prior distribution on the parameters. Firstly, in the Bayesian framework, the prior is an integral part of the model, since Bayesian inference automatically yields the *updated* results with respect to prior knowledge. Secondly, the concept of predictability or complexity of a model makes sense only in comparison with the model prior; this is the core of the Lindley-Jeffrey paradox (Lindley 1957) which is illustrated nicely in Trotta (2007). In short, a model is penalised if it requires fine-tuning of parameters, corresponding to a posterior distribution that is very concentrated in terms of the prior mass. (Efstathiou 2008). As Efstathiou (2008) pointed out, the lack of a physically well-motivated model and therefore the choice of an ad-hoc prior will strongly decrease the usefulness of a model selection analysis. Since fundamental physical understanding is often lacking in cosmology, the application of the Bayesian evidence might indeed be limited. However, we should not consider this as a fallacy of Bayesian inference but rather take it as a motivation to find well-defined physical models which can be compared in a sensible way (Trotta 2008).

2.3 Estimating the Bayesian evidence with importance sampling

We propose to estimate the evidence using importance sampling (IS). IS provides a converging approximation of the integral (1) as follows. For a probability density function q whose support includes that of the posterior π , we can transform (1) as

$$E = \int \pi(x) dx = \int \frac{\pi(x)}{q(x)} q(x) dx. \quad (3)$$

IS performs a Monte-Carlo integration of E by drawing N samples x_1, \dots, x_N from the *importance function* q to approximate E with the sample average

$$E \approx \frac{1}{N} \sum_{n=1}^N w_n; \quad w_n = \frac{\pi(x_n)}{q(x_n)}, \quad (4)$$

where the w_n are called (unnormalised) importance weights. For later use, we introduce their normalised counterparts, marked with a bar,

$$\bar{w}_n = \frac{w_n}{\sum_{m=1}^N w_m}. \quad (5)$$

Of course, the quality of the estimate (4) of E depends on the choice of the importance function q . The variance of (4) is

$$\sigma_E^2 = \frac{E^2}{N} d^2(\bar{\pi}||q), \quad (6)$$

with the so-called chi-square distance

$$d^2(\bar{\pi}||q) = \int \frac{\bar{\pi}^2(x)}{q(x)} dx - 1. \quad (7)$$

Therefore, a suitable choice of q is such that $d^2(\bar{\pi}||q)$ is as small as possible. In practise, this means that for each specific problem (i.e., each specific π), efficient importance functions have to be found, which is a non-trivial task. Hence the appeal of *adaptive* IS methods which rely on numerical optimization schemes that can automatically select a suitable q . Except in particular cases (Douc et al. 2007), it is quite hard to devise computationally efficient adaptive schemes based on the (7) distance and we discuss below an algorithm that targets a alternative measure of fit between $\bar{\pi}$ and q .

2.4 Adaptive importance sampling

Population Monte Carlo tackles the problem of the importance function choice by an adaptive solution: The PMC algorithm produces a sequence q^t , $t = 1, \dots, T$ of importance functions aimed at progressively approximating the posterior π .

The quality of approximation is measured in terms of the Kullback-Leibler divergence (Kullback & Leibler 1951; Cover & Thomas 1991) from the posterior,

$$K(\bar{\pi}||q^t) = \int \log \left(\frac{\bar{\pi}(x)}{q^t(x)} \right) \bar{\pi}(x) dx, \quad (8)$$

rather than the chi-square distance (7), and the density q^t can be adjusted incrementally to minimize this divergence. Note that the optimisation algorithm is independent of the normalisation of the posterior. Therefore, for all practical purposes, the unnormalised posterior π can be used in (8).

The importance function should be selected from a family of functions which is sufficiently large to allow for a close match with $\bar{\pi}$ but for which the minimization of (8) is computationally feasible. Cappé et al. (2008) propose to use mixture densities of the form

$$q^t(x) = q(x; \alpha^t, \theta^t) = \sum_{d=1}^D \alpha_d^t \varphi(x; \theta_d^t), \quad (9)$$

where $\alpha^t = (\alpha_1^t, \dots, \alpha_D^t)$ is a vector of adaptable weights for the D mixture components (with $\alpha_d^t > 0$ and $\sum_{d=1}^D \alpha_d^t = 1$),

and $\theta^t = (\theta_1^t, \dots, \theta_D^t)$ is a vector of parameters which specify the components; φ is a parametrized probability density function, usually taken to be multivariate Gaussian or Student-t. This choice of the importance function is very flexible and allows to approximate a wide range of posteriors.

The first sample in this adaptive scheme is produced by a regular importance sampling mechanism, $x_1^1, \dots, x_N^1 \sim q^1$, associated with importance weights

$$w_n^1 = \frac{\pi(x_n^1)}{q^1(x_n^1)}; \quad n = 1, \dots, N, \quad (10)$$

providing a first approximation to a sample from π .

At each stage t of the iteration, the sample points and weights from that iteration, $(x_1^t, w_1^t), \dots, (x_N^t, w_N^t)$, are used to update the importance function q^t to the new one, q^{t+1} . During the next iteration, a new sample $x_1^{t+1}, \dots, x_N^{t+1}$ is then drawn from the updated importance function q^{t+1} .

The updating method is based on a variant of the Expectation-Maximization algorithm (EM, Dempster et al. 1977). New parameters $\alpha^{t+1}, \theta^{t+1}$ are obtained by carrying out an IS approximation of the update of the EM algorithm to obtain a reduction in the Kullback-Leibler divergence (8).

As an illustration of a simple updating rule, the new weights of the mixture components can be calculated according to

$$\alpha_d^{t+1} = \sum_{n=1}^N \bar{w}_n^t 1_d(x_n^t). \quad (11)$$

Here, $1_d(x)$ denotes the d^{th} -component indicator function which is unity if x has been drawn from component d , and zero otherwise. The updated component weight α_d^{t+1} is thus the sum of the normalized importance weights of the sample points drawn from the d^{th} component, leading to a simple intuition of the adaptation. Points sampled from a component which approximates the posterior well (badly) have large (small) weights, and the component will be up-weighted (down-weighted) in the update. Note that in our implementation of PMC we use improved and more robust versions of this updating rule. Details of the algorithm as well as formulae and their derivations for updating the mean and covariance in the case of Gaussian and Student-t mixtures are given in Cappé et al. (2008) and WKB09.

2.5 Diagnostics

Although a formal stopping rule for the above described iterative process does not exist, performance measures can be defined to serve as guidelines. As PMC aims at minimizing the Kullback-Leibler divergence K (8) across iterations, one can stop the process when subsequent importance functions do not yield a significant decrease of K . We estimate $\exp[-K(\bar{\pi}||q^t)]$ by the *perplexity*

$$p = \exp(H_N^t)/N, \quad (12)$$

where

$$H_N^t = - \sum_{n=1}^N \bar{w}_n^t \log \bar{w}_n^t \quad (13)$$

is the Shannon entropy of the normalised weights. Values of p close to unity will therefore indicate good agreement between the importance function and the posterior.

Another frequently used criterion for importance sampling is the so-called *effective sample size* (ESS),

$$\text{ESS}_N^t = \left(\sum_{n=1}^N \{\bar{w}_n^t\}^2 \right)^{-1}, \quad (14)$$

with $1 \leq \text{ESS}_N^t \leq N$. The effective sample size can be interpreted as the number of sample points with non-zero weight (Liu & Chen 1995). Both measures (12, 14) are related, as an importance function which is close to the posterior density will in general have both a high perplexity and a relatively large number of points with non-zero weight, compared to an ill-fitting importance function.

2.6 The initial proposal

The efficiency of the algorithm is dependent on the initial choice of the proposal. A poor initial importance function, e.g. a single-mode function in the case of a multimodal posterior or a too narrow function with light tails, may take a very long time to adapt or even miss important parts of the posterior. For importance sampling the choice of q requires both fat tails and a reasonable match between q and the posterior π in regions of high density. Such an importance function can be more easily constructed in the presence of a well-informed guess about the parameters and possibly the shape of the posterior density. In our application of PMC to cosmology (Sect. 4) we will use the Fisher matrix as an aid for the initial proposal.

2.7 Summary

PMC offers a fast and reliable way to estimate the Bayesian evidence, see eq. (4), with an expression of the variance of this estimator provided by (6). Diagnostics of the reliability of the sampling are at hand. The evaluations of the likelihood function can further be massively parallelized with importance sampling, offering an enormous decrease of the required wall-clock time to obtain the evidence. This feature is unique to importance sampling techniques and thus not partaken by alternative techniques such as nested sampling and MCMC. We stress again that the calculation of the evidence comes at virtually no further computation cost than parameter estimation using PMC.

3 SIMULATIONS

In this section we use simulated data and a toy model for the posterior density to assess the performance of the PMC approach to provide an accurate estimate of the evidence. We use a non-Gaussian posterior density, twisting a centred d -dimensional multivariate Gaussian in the first two dimensions. One can easily build a sample under this twisted posterior distribution, using

$$x' = (x'_1, x'_2, \dots, x'_d) \sim \mathcal{N}_d(0, \Sigma), \quad (15)$$

where $\Sigma = \text{diag}(\sigma_1^2, 1, \dots, 1)$ is the covariance, and transforming it to

$$x = (x'_1, x'_2 - \beta(x'_1)^2 - \sigma_1^2, x'_3, \dots, x'_d). \quad (16)$$

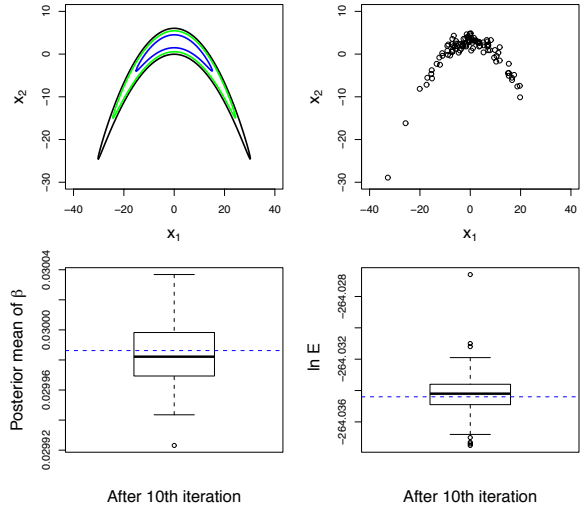


Figure 1. *Top panels:* The posterior distribution (16) for $\beta = 0.03$, with the true 68.3% (blue), 95% (green), and 99.7% (black) density contours (*left*) and $M = 100$ simulated data points drawn from (16), both shown in the first two dimensions. *Bottom panels:* Estimates over 100 simulation runs after the 10th iteration of β (*left*), and the Bayesian evidence (*right*). The distributions are shown as whisker plots: the thick horizontal line represents the median; the box shows the interquartile range (IQR), containing 50% of the points; the whiskers indicate the interval $1.5 \times \text{IQR}$ from either Q1 (lower) or Q3 (upper); points outside the interval $[Q1, Q3]$ (outliers) are represented as circles. Posterior means of E and β from the simulated data are indicated as dashed lines.

The twist parameter β controls the degree of curvature. This example was also used in WKB09 to assess the performance of PMC for parameter estimation. In the following, we will use $d = 5$ and $\sigma_1^2 = 100$.

3.1 Unknown twist β

As a first benchmark, our interest is in estimating β and in obtaining the evidence E by integrating out β from the unnormalised posterior distribution, i.e.

$$E = \int \pi(\beta|x, \Sigma) d\beta. \quad (17)$$

As β is a scalar we can easily calculate (using a grid-point or adaptive quadrature approach) the evidence by integrating over this one-dimensional domain.

For this example we take a simulated data set x with size $M = 100$, and input twist $\beta = 0.03$. Fig. 1 shows the confidence contours of the posterior density defined by eq. (16) (top left panel) and the simulated data points (top right) in the first two dimensions. From eq. (16), the likelihood is defined as

$$L(\beta) = \prod_{m=1}^M \frac{1}{(2\pi)^{d/2} |\Sigma|^{1/2}} \exp(-0.5 x_m^T \Sigma^{-1} x_m), \quad (18)$$

where each $x_m = (x_{m1}, x_{m2} + \beta(x_{m1}^2 - \sigma_1^2), x_{m3}, \dots, x_{md})$ is a transformed sample point according to (16). Note that the Jacobian of the transformation is unity. The prior for β is uniform on the unit interval, $P(\beta) = U(0, 1)$.

The initial importance function q^1 was chosen to be a mixture of three Gaussian distributions with means randomly displaced around zero and variance 0.5, allowing for a somewhat vague initial coverage of the parameter space. For the results to follow the number of points at each PMC iteration was $N = 1000$, with a number of PMC iterations equal to $T = 10$. To assess the variability and distribution of the results we repeated this process 100 times. Fig. 1 shows the estimates of β (bottom left) and the evidence (bottom right) over the 100 simulation runs after the 10th iteration. We find for the mean and 68% confidence $\beta = 0.02998 \pm 0.00002$ and $\ln E = -264.0342 \pm 0.0010$. Comparing these results to the posterior mean values corresponding to the sample of $M = 100$ simulated data points, $\beta = 0.0299862$ and $\ln E = -264.0344$ suggests that PMC performs very well in providing an accurate estimate of the evidence and of β .

3.2 Known twist β

For the second case, we use the slightly twisted centred multivariate Gaussian as before but this time β is known, $\beta = 0.015$, and we integrate over the posterior represented by (16), i.e.

$$E = \int \pi(x|\beta, \Sigma) dx \quad (19)$$

is our target. This presents a much more difficult exercise with the tails of the posterior being a significant challenge to capture, and the dimension of the space to be integrated over is $d = 5$. To estimate the evidence with PMC in this second example, the number of points at each iteration was $N = 10000$, the number of PMC iterations $T = 10$ and as in the first example we use 100 simulation runs to assess the variability of the estimates. After the 10th iteration we draw a final sample of size $N = 100,000$. The initial importance function q^1 is a mixture of multivariate Student-t distributions with components displaced randomly in different directions slightly away from the centre of the range for each variable: the mean of the components is drawn from a p-multivariate Gaussian with mean 0 and covariance equal to $\Sigma_0/5$ where Σ_0 is the covariance of the proposal components. We choose a mixture of 9 components of Student-t distribution with $\nu = 9$ degrees of freedom; and Σ_0 is a diagonal matrix with diagonal entries (200, 50, 4, ..., 4). This choice of (ν, Σ_0) ensures adequate coverage, albeit somewhat overdispersed, of the feasible parameter region.

Fig. 2 shows the estimates of the evidence (bottom right) against the true value over the 100 simulation runs after the 10th iteration.

The results for this more difficult case suggest that PMC performs reasonably well in providing an accurate determination of the evidence. The estimates at each iteration (Fig. 2, bottom left) are stable, with a reduction in the variability seen as the importance function better adapts to the posterior density. The adaptation performance can be seen by the increase in estimates of the normalized perplexity and effective sample size (Fig. 2, top right) for successive iterations. See fig. 1 of WKB09 for a graphical example of the adaptation of the importance function to the posterior for $d = 10$. After the final iteration (Fig. 2, bottom right), the estimate of the evidence is $\ln E = -0.0019 \pm 0.0038$ at 68% confidence. The presence of a slight downward bias from the

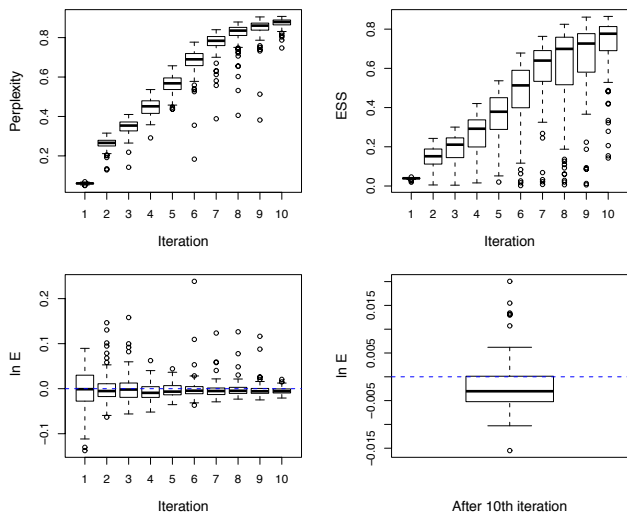


Figure 2. PMC sampling of (16) as a function of iteration over 100 simulation runs. *Top left:* Estimates of the perplexity (12); *Top right:* Effective sample size (14); both normalized by N . *Bottom:* Estimates of the evidence at each iteration (*left*), and after the 10th iteration using $N = 100,000$ sample points (*right*). The true value 0 is indicated as a dashed line. See Fig. 1 for details about the whisker plot representation.

true value of zero is not unexpected due to the use of the log-scale (as a consequence of Jensen’s inequality, an unbiased estimate of E would look biased when plotted on the log-scale). This could also be due to the importance function not fully exploring the low probability tails of the posterior density. However in the case of Fig. 2, the bias in terms of the scale is very small, and is associated with equally small variability of the estimates of E .

4 COSMOLOGY

The so-called standard model of cosmology is successful in explaining recent observations of cosmology, such as the CMB, supernovae of type Ia (SNIa), galaxy clustering including baryonic acoustic oscillations (BAO), cosmic shear, galaxy cluster counts, and Ly α forest clustering. This flat Λ CDM model has only six free parameters ($\Omega_m, \Omega_b, h, n_s, \tau, \sigma_8$, or functions thereof) and is therefore surprisingly simple.

Despite this, various extensions to the standard model are considered and tested routinely using observational data. These extensions may be based on independent evidence (for example massive neutrinos from oscillation experiments), be predicted by a compelling hypothesis (primordial gravitational waves from inflation) or reflect our ignorance about the fundamental physics (dynamical dark energy). Whatever be the case, future surveys and analyses are to answer the question which of the many models is the one to best describe the observations. So far, no extension of the standard model has been strongly supported by the data.

In this paper, we use the Bayesian evidence as a tool to compare different models and their ability to describe cosmological data. As described in Sect. 2.3, we use PMC to

sample the posterior and to calculate the evidence. We take recent data of CMB (Hinshaw et al. 2009), SNIa (Kowalski et al. 2008) and BAO (Eisenstein et al. 2005). The extensions to the standard model of cosmology concern dark energy and curvature (Sect. 4.2), and inflationary models (Sect. 4.3).

4.1 PMC set-up

To set up PMC we have to choose the initial proposal, q^1 , the number of sample points, N , and the number of iterations, T . We take q^1 to be a Gaussian mixture model with D components, which are displaced from the maximum-likelihood point by a random shift f_{shift} in each dimension, with f_{shift} being the fraction of the prior parameter range. The covariance of the components corresponds to the Fisher matrix rescaled by a number f_{var} , typically of order unity, or larger if the Fisher matrix is suspected to be significantly narrower than the posterior curvature.

For the dark-energy and curvature models (Sect. 4.2), we choose the number of iterations T to be 10. If after 10 iterations the perplexity is still low, say, smaller than 0.6, we run PMC for more iterations. The choices of the N and D are linked: the average number of points sampled under an individual mixture-component, N/D , should not be too small, to ensure a numerically stable updating of this component. We choose $N = 7500$ and $D = 10$.

For the primordial models (Sect. 4.3) we take $T = 5$, $N = 10000$ and D between 7 and 10, depending on the dimensionality and shape of the likelihood.

The parameters controlling the initial mixture means and covariances, are chosen for both cases to be $f_{\text{shift}} = 0.02$, and f_{var} between 1 and 1.5. For the final iteration we choose a five-times larger sample than for previous iterations.

4.2 Dark energy and curvature

Here we test the standard Λ CDM-model assumptions of a cosmological constant and flatness. We parametrize the dark energy equation-of-state parameter as constant and as linear function in the scale factor a , respectively. Together with the basic model for which $w = -1$, we compare the three cases:

$$\begin{aligned} w = -1 & & \Lambda\text{CDM} \\ w = w_0 & & w\text{CDM} \\ w = w_0 + w_1(1 - a) & & w(z)\text{CDM} \end{aligned} \quad (20)$$

In addition, the curvature parameter Ω_K for each of the above models is either $\Omega_K = 0$ ('flat') or $\Omega_K \neq 0$ ('curved').

We do not take into account dark energy clustering. The observational data is reduced to purely geometrical probes of the Universe; for CMB these are the distance priors (Komatsu et al. 2009) and for BAO the distance parameter A (Eisenstein et al. 2005). The common parameters for all models are Ω_m , Ω_b and h . All models share the same flat priors for those three parameters; the prior ranges for all parameters can be found in Table 2. We verified that the relative evidence between models, or Bayes factor, does not depend on the prior ranges for nested parameters if the high-density likelihood region is situated far from the prior boundaries.

Table 2. Prior ranges for dark energy and curvature models. In case of $w(a)$ models, the prior on w_1 depends on w_0 , see Sect. 4.2.1.

Parameter	Description	Min.	Max.
Ω_m	Total matter density	0.15	0.45
Ω_b	Baryon density	0.01	0.08
h	Hubble parameter	0.5	0.9
Ω_K	Curvature	-1	1
w_0	Constant dark-energy par.	-1	-1/3
w_1	Linear dark-energy par.	-1 - w_0	$\frac{-1/3 - w_0}{1 - a_{\text{acc}}}$

4.2.1 Dark-energy prior

The simple parametrization of w clearly is not motivated by fundamental physics of dark energy. However, this choice represents the most simple models which go beyond a cosmological constant; it makes therefore sense to use those extensions in a model-selection framework. To define a physically sound prior of these dark-energy parameters, we restrict ourselves to a specific class of models. Our goal is to find a model which is able to explain the observed, recent accelerated expansion of the Universe. The model should therefore include a component to the matter-density tensor with $w(a) < -1/3$ for values of the scale factor $a > a_{\text{acc}}$. We choose $a_{\text{acc}} = 2/3$. To limit the equation of state from below, we impose the condition $w(a) > -1$ for all a , thereby excluding phantom energy as in Efstathiou (2008). Fig. 4 shows the allowed range in the case of two dark-energy parameters. We note that our approach is inconsistent to some extent in that the data on which the observation of accelerated expansion is based on is part of the data used in this analysis.

4.2.2 Curvature prior

A natural limit on the curvature is that of an empty Universe; this certainly places an upper boundary on the curvature, corresponding to $\Omega_K = 1$. A lower boundary, corresponding to an upper limit on the total matter-energy density, is less stringent. We choose $\Omega_K > -1$; this 'astronomer's prior' (Vardanyan et al. 2009) provides a symmetric prior around the null-hypothesis value and excludes high-density Universes which are ruled out by the age of the oldest observed objects.

An alternative prior on Ω_K could be derived from the paradigm of inflation. However, most inflationary scenarios imply the curvature to be extremely close to zero, on the order of 10^{-60} . The likelihood over such a prior on Ω_K is essentially flat for any current and future (Waterhouse & Zibin 2008) experiment. A model with such an uninformative likelihood would be indistinguishable in terms of the Bayesian evidence with respect to a flat model.

4.2.3 Results

In Fig. 3 we plot the Bayes factor for various models with respect to the standard flat Λ CDM model. In most cases there is positive evidence in favour of the standard model. This evidence against more complex models increases if more probes are combined. This is not surprising: no deviation

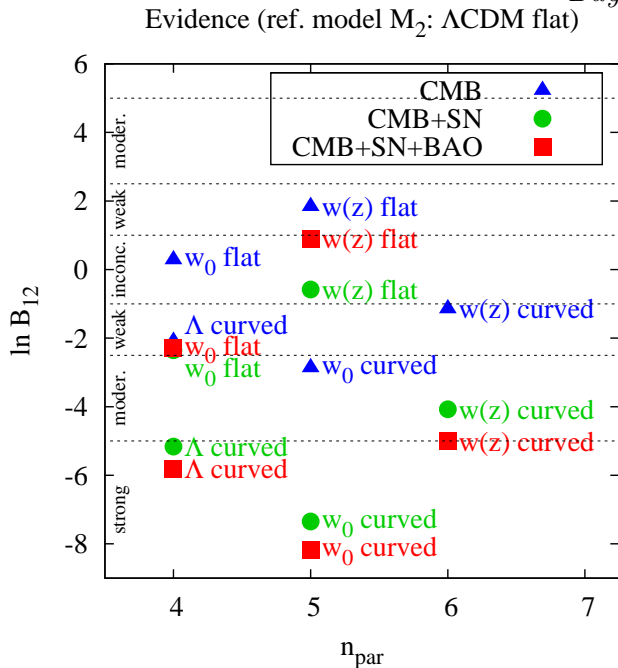


Figure 3. Evidence for various models \mathfrak{M}_1 with respect to the reference flat Λ CDM model \mathfrak{M}_2 with $n_{\text{par}} = 3$. The different combinations of data are CMB (blue triangles), CMB+SNIa (green circles) and CMB+SNIa+BAO (red squares). Note that the Bayes factor between different non-reference models can only be compared for the same combination of data (same symbols).

from $w = -1$ and $\Omega_K = 0$ has been found, additional parameters are not supported by the data. The more data are added, the tighter get the constraints around the standard values, therefore the stronger gets the evidence in favour of this simplest model.

The largest positive evidence is $\ln B_{12} = 1.8$, for the $w(z)$ CDM model and CMB alone. In this case, as can be seen in Fig. 4, a large part of the prior range is still allowed by the data, and a region of comparable size is excluded. There is weak evidence that the two extra-parameters w_0 and w_1 are indeed required by the data. When adding SNIa and BAO, most of the prior range is excluded, and this ‘waste’ of parameter space is penalised by decreasing the Bayes factor.

Regarding the prior on w_0 , our w CDM model corresponds to Model II from Serra et al. (2007). In that work, SN data alone led to a $\ln B_{12}$ of around -0.2 (comparing Λ CDM to Model II). In our case, the combination of SN with CMB and BAO leads to a larger evidence in favour of Λ CDM.

Our results on the curvature are compatible with the findings of Vardanyan et al. (2009). Using all three data sets, a non-flat Universe is strongly disfavoured for all three dark-energy cases. For comparison, Vardanyan et al. (2009) showed that using a flat prior in $\log \Omega_K$, corresponding to a flat prior on the curvature *scale*, therefore largely increasing the prior volume, leads to inconclusive evidence.

4.2.4 Stability of the results

We test the reliability of the results for two of the cases presented in Sect. 4.2, w CDM flat and w CDM curved, both using CMB+SN+BAO data. We repeat the PMC runs 25

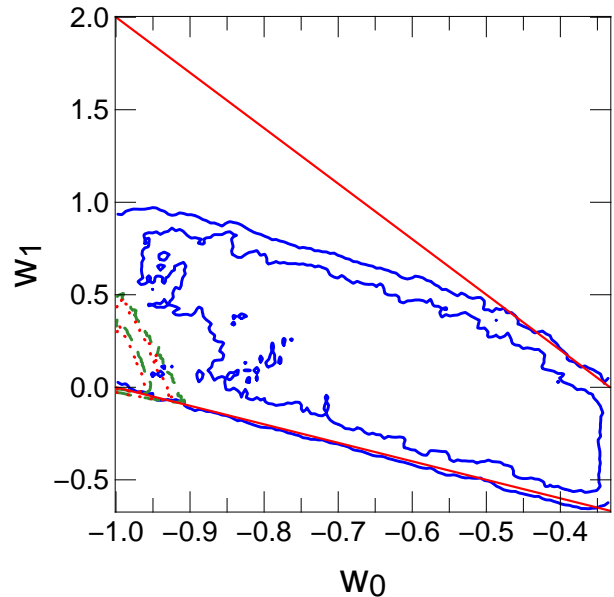


Figure 4. 68%- and 95% confidence regions for WMAP (solid blue lines), WMAP+SNIa (dashed green) and WMAP+SNIa+BAO (dotted red curves). The allowed range for the dark-energy parameters w_0 and w_1 lies between the two red straight lines.

times. For a given scheme with fixed proposal parameters f_{shift} , f_{var} and D (Sect. 4.1), we randomly vary the positions and widths of the initial proposal components.

The distribution of the log-evidence $\ln E$ and the normalized perplexity is shown in Fig. 5 for two cases of dark-energy models. Since the components of the proposal move towards the tails of the posterior with progressing iteration, the evidence keeps on increasing with better sampling of the tails. The high value at the first iteration is biased and dominated by a few points with very large importance weights $w_n = \pi(x_n)/q(x_n)$, which are sampled from the proposal tails but lie in regions of high posterior density $\bar{\pi}$.

For the flat w CDM model the evidence converges after a few iterations showing a very small dispersion between runs with $\ln E = -9.159 \pm 0.011$ (68% confidence) at $t = 10$. The relatively large perplexity of $p \approx 0.6 - 0.7$ indicates a reliable sampling of the posterior. The posterior of the curved model is more elongated which makes the sampling more difficult. The perplexity does not exceed 0.4 even after 20 iterations. The evidence however stabilises onto a narrow interval after ~ 18 iterations, $\ln E = -10.84 \pm 0.077$ (68% confidence) at $t = 20$.

4.3 Primordial perturbations

In the following, we test models corresponding to various descriptions and parametrizations of primordial fluctuations. The (dark-matter) density fluctuations are given by the power spectrum as function of scale k ,

$$P_\delta(k) \propto k^{n_s + \frac{1}{2} \alpha_s \ln(k/k_0)}, \quad (21)$$

with the parameters n_s being the scalar spectral index, and α_s the ‘running’ of the index, i.e. the first-order Taylor term of the exponent. The pivot scale k_0 is fixed to

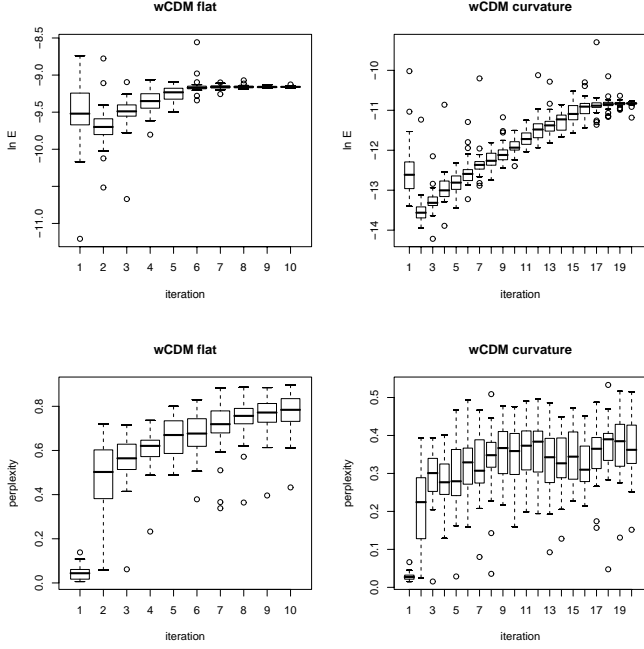


Figure 5. Distribution of 25 PMC samplings of two dark-energy models, flat w CDM (*left panels*) and curved w CDM (*right panels*). *Top (Bottom)*: The log-evidence (perplexity) as function of iteration. See Fig. 1 for details about the whisker plot representation.

$k_* = 0.002 \text{ Mpc}^{-1}$. In addition, tensor-modes (gravitational waves) have the power spectrum

$$P_t(k) \propto k^{n_t}, \quad (22)$$

with tensor spectral index n_t . The ratio between tensor and scalar perturbation spectra at scale k_0 is denoted by r . In the standard model, $\alpha_s = n_t = r = 0$, only n_s is a free parameter. Most inflationary models predict n_s to be slightly below unity, therefore the power spectrum of primordial density perturbations is a near scale-free power law. Tensor perturbations (gravitational waves) are expected to be non-zero, but their amplitude is unknown and current data have not been able to detect those modes.

Although tensor-modes are expected from most models of the early Universe, they are not detected so far with the given sensitivity of current data.

The models we consider for our Bayesian evidence analysis are interpreted within the slow-roll approximation of inflation, as will be described in the next section.

4.3.1 Slow-roll parameters

The slow-roll approximation of inflation provides an infinite hierarchy of flow equations describing the dynamics of the single scalar field which drives inflation (see Peiris & Easter 2006, and references therein). The slow-roll parameters ϵ and ${}^\ell\lambda_H, \ell \leq 1$ are defined in terms of the potential V of the scalar field ϕ , and the Hubble parameter H ,

$$\epsilon = \frac{m_{\text{Pl}}^2}{4\pi} \left[\frac{H'}{H} \right]^2; \quad (23)$$

$${}^\ell\lambda_H = \left(\frac{m_{\text{Pl}}^2}{4\pi} \right)^\ell \frac{(H')^{\ell-1}}{H^\ell} \frac{d^{\ell+1}H}{d\phi^{\ell+1}}; \ell \leq 1, \quad (24)$$

Table 3. Prior ranges for primordial model comparison. The prior ranges for primordial parameters are derived from the slow-roll approximation.

Parameter	Description	Min.	Max.
Ω_m	Total matter density	0.01	0.6
Ω_b	Baryon density	0.01	0.1
τ	Reionisation optical depth	0.01	0.3
$10^9 \Delta_{\mathcal{R}}^2$	Normalisation	1.4	3.5
h	Hubble parameter	0.2	1.4
n_s	Scalar spectral index	0.39	1.2
α_s	Running of spectral index	-0.2	0.033
r (lin. prior)	Tensor-to-scalar ratio	0	1.65
$\ln r$ (log. prior)	Tensor-to-scalar ratio	-80	0.50

where the prime denotes derivation with respect to ϕ . The Planck mass is denoted by m_{Pl} . The hierarchy of flow parameters can be truncated, since if some ${}^L\lambda_H = 0$, all higher terms ${}^\ell\lambda_H, \ell > L$ vanish. We consider the expansion up to first-order and set ${}^1\lambda_H = \eta, {}^2\lambda_H = 0$. The parameters of the primordial power spectra can be written in terms of the slow-roll parameters as

$$n_s = 1 + 2\eta - 4\epsilon - 2(1 + \mathcal{C})\epsilon^2 - \frac{1}{2}(3 - 5\mathcal{C})\epsilon\eta; \quad (25)$$

$$r = 16\epsilon [1 + 2\mathcal{C}(\epsilon - \eta)]; \quad (26)$$

$$\alpha_s = \frac{\epsilon}{1 - \epsilon} (10\eta - 8\epsilon); \quad (27)$$

$$n_t = -2\epsilon - (3 + \mathcal{C})\epsilon^2 + (1 + \mathcal{C})\epsilon\eta. \quad (28)$$

Here, $\mathcal{C} = 4(\ln 2 + \gamma) - 5 \approx 0.0814514$ where $\gamma = 0.577216$ is the Euler-Mascheroni constant. For slow-roll inflation to take place, the slow-roll conditions $\epsilon \ll 1$ and $|{}^\ell\lambda_H| \ll 1$ for all ℓ have to be satisfied.

4.3.2 Priors

We use the slow-roll conditions to define priors on the primordial parameters as $0 \leq \epsilon \leq 0.1$ and $|\eta| \leq 0.1$. Although the exact values of the prior boundaries are somewhat arbitrary, they have been considered by Martin & Ringeval (2006) as natural limits for the validity of the Taylor-expansion of the power spectrum $P(k)$ in $\ln(k/k_*)$ around the pivot scale $k_* = 0.05 \text{ Mpc}^{-1}$. We use $k_* = 0.002 \text{ Mpc}^{-1}$ as pivot, in accordance to the WMAP5 analysis; we verified the equivalence of our results for both cases of k_* . We choose an uninformative (i.e. flat) prior on the slow-roll parameters. From eqs. (25-28) we get the corresponding ranges of the power-spectra parameters, see Table 3, which are now motivated from fundamental physical principles within the slow-roll model of inflation. We choose flat priors for the power-spectra parameters as well, although they are nonlinearly related to the slow-roll parameters and the prior will have a different shape. However, we ignore this for simplicity. See Trotta (2007) for a similar approach to define a prior on the spectral index tilt. The tensor index n_t is unconstrained by current data; therefore, we do not include this parameter.

We compare various models to the standard paradigm, which now has six parameters ($\Omega_m, \Omega_b, h, n_s, 10^9 \Delta_{\mathcal{R}}^2, \tau$). For our model testing, we single out individual parameters or combinations thereof. A strictly consistent and thorough

treatment should treat the slow-roll parameters as primary parameters; this will be left for a future analysis.

4.3.3 Results

In Fig. 6 we show the Bayes factor of various models \mathfrak{M}_1 with respect to the standard model \mathfrak{M}_2 , a flat Λ CDM Universe with $n_s = \text{const}$. A running spectral index is favoured weakly, all other cases are disfavoured. The evidence against the Harrison-Zel'dovich model ($n_s = 1$) is weak, whereas tensor perturbations are moderately disfavoured. For illustration, we include a tensor-mode model with flat prior for $\ln r$ instead of r ; the minimum is chosen to be -80 , corresponding to the Planck length as energy scale of inflation (Parkinson et al. 2006). The large prior of the logarithmic tensor-to-scalar ratio causes this model to be strongly disfavoured. Note however that this example is not consistent with flat priors for the slow-roll parameters; it rather corresponds to a model in which very small slow-roll parameters are much more likely than large ones.

Previous results showed both positive as well as negative evidence for a scale-free, Harrison-Zel'dovich spectrum compared to a tilted power law (Bridges et al. 2006; Mukherjee et al. 2006; Bridges et al. 2007; Trotta 2007). The evidence in either direction is however moderate at most. More narrow priors on n_s increase the evidence for the HZ model. Our result is in agreement with those previous works, taken into account the differences in the employed data and priors. This shows that the evidence against a scale-free spectrum is not yet substantial with the current data, and it calls for physically motivated prior density.

Previous results showed positive and negative evidence for a non-zero running of the spectral index α_s , depending on the prior width (Bridges et al. 2007). Our positive value of $+1.73$ is relatively high but still corresponds to only weak evidence in favour of $\alpha_s \neq 0$.

5 CONCLUSION

The Bayesian evidence E provides a mathematically consistent and intuitive tool to compare different models and to choose between competing models. Its calculation in high-dimensional parameter spaces is in general numerically challenging, as the posterior distribution may be multimodal and/or show strong non-linear parameter-dependencies.

Simplification methods such as the Laplace approximation are not sufficient and cannot replace the full integration of the posterior over the parameter space. Laplace assumes a multivariate (i.e. single-peaked) Gaussian likelihood and a prior which is much wider than the likelihood. If either of these assumptions is violated, the approximation can give values of $\ln E$ which are wrong by several dex. Although in many cases the likelihood might be close to Gaussian, or can be brought in such a form by parameter transformations, this is not possible in general, and often there exist hard, physical priors which cut off the likelihood.

In this paper, we use Population Monte Carlo (PMC) to estimate the Bayesian evidence. PMC is a new, adaptive importance sampling method which offers an efficient and reliable way to obtain the Bayesian evidence for non-trivial

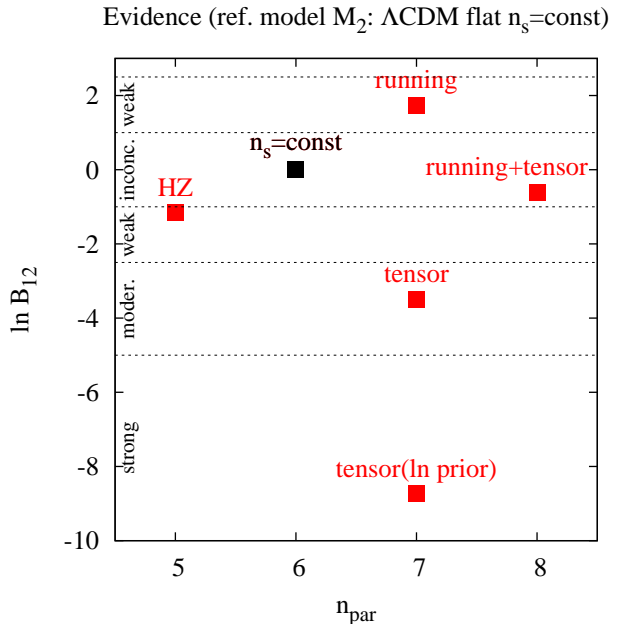


Figure 6. Evidence for various models \mathfrak{M}_1 with respect to the reference model \mathfrak{M}_2 , a flat Λ CDM Universe with constant n_s .

likelihood shapes. An expression for the variance of the evidence estimator is introduced. We will leave a study of an estimator of this variance for future work. Here, we repeat PMC runs to study the distribution of the evidence, and show the robustness of the results. If the initial proposal is badly chosen the estimate of E can be significantly off; such cases can however be identified by the in-built diagnostic tools of PMC, e.g. the perplexity and effective sample size.

Other methods to estimate the Bayesian evidence have been proposed, e.g. VEGAS (Lepage 1978; Serra et al. 2007) which necessitates that the likelihood function can be brought into a separable form. Another computationally efficient since to some extent parallelizable algorithm is (multi-)nested sampling (Skilling 2006; Feroz & Hobson 2008; Feroz et al. 2009). While being a special case of importance sampling (Robert & Wraith 2009), nested sampling draws from the prior instead from an importance function approximating the posterior as in PMC. See Clyde et al. (2007); Marin & Robert (2010) and Robert & Wraith (2009) for an overview of various methods of Bayesian evidence estimation including Markov chain Monte Carlo methods.

We have applied Bayesian model selection to two domains of cosmology, the accelerated expansion of the Universe in the recent past and primordial fluctuations in the early Universe. For the former, we analysed simple, parametrized models of dark energy; the latter used the slow-roll approximation of inflation. We employed recent cosmological data corresponding to CMB, SNIa and BAO.

No dark-energy model is strongly or even only moderately favoured over the standard Λ CDM paradigm. This is in spite of the rather strong prior on dark-energy, i.e. excluding phantom energy and requiring an accelerating component in the recent past. More general dark-energy models with larger parameter spaces will likely be disfavoured with respect to Λ CDM. This is even true if future experiments find

deviations of w from -1 unless the error bars get extremely small (Lindley-Jeffrey paradox). This should serve as a motivation to define a tight physical framework for dark-energy models with stronger prior constraints on parameters.

We find strong evidence against a non-flat Universe using the combined CMB+SNIa+BAO data. This is true regardless of the chosen dark-energy model. It holds for a prior belief that $|\Omega_K| \leq 1$.

We use a natural limit on slow-roll inflation parameters to deduce prior ranges for the primordial perturbation spectra parameters. The preferred model contains a non-zero running spectral index ($\alpha_s \neq 0$) and no tensor modes ($r = 0$). The evidence is however only weak. A scale-free, Harrison-Zel'dovich model is weakly disfavoured. Tensor modes are moderately to strongly disfavoured, depending on the prior shape on r . As a consequence, future detections of tensor modes have to be done with very high significance, to strongly disfavour a $r = 0$ model.

ACKNOWLEDGMENTS

We would like to thank Jean-Francois Giovannelli and Jean-Phillip Uzan for fruitful discussions. We acknowledge the use of the Legacy Archive for Microwave Background Data Analysis (LAMBDA). Support for LAMBDA is provided by the NASA Office of Space Science. We thank the Planck group at IAP and the TERAPIX group for support and computational facilities. MK and DW are supported by the CNRS ANR 'ECOSSTAT', contract number ANR-05-BLAN-0283-04 ANR ECOSSTAT. This project is partly supported by the Chinese National Science Foundation Nos. 10878003 & 10778725, 973 Program No. 2007CB 815402, Shanghai Science Foundations and Leading Academic Discipline Project of Shanghai Normal University (DZL805).

This paper has been typeset from a $\text{\TeX}/\text{\LaTeX}$ file prepared by the author.

REFERENCES

- Akaike H., 1974, IEEE Transactions on Automatic Control, AC-19, 716
- Benabed K., Cardoso J., Prunet S., Hivon E., 2009, MNRAS, 400, 219
- Berger J., Jeffreys W., 1992, Amer. Statistician, 80, 64
- Bridges M., Lasenby A. N., Hobson M. P., 2006, MNRAS, 369, 1123
- Bridges M., Lasenby A. N., Hobson M. P., 2007, MNRAS, 381, 68
- Cappé O., Douc R., Guillin A., Marin J.-M., Robert C., 2008, Statist. Comput., 18(4), 447
- Cappé O., Guillin A., Marin J.-M., Robert C., 2004, J. Comput. Graph. Statist., 13, 907
- Chen M., Shao Q., Ibrahim J., 2000, Monte Carlo Methods in Bayesian Computation. Springer
- Clyde M. A., Berger J. O., Bullard F., Ford E. B., Jefferys W. H., Luo R., Paulo R., Loredo T., 2007, in Babu G. J., Feigelson E. D., eds, Statistical Challenges in Modern Astronomy IV Vol. 371 of Astronomical Society of the Pacific Conference Series. p. 224
- Cover T. M., Thomas J. A., 1991, Elements of information theory. John Wiley and Sons, Inc.
- Dempster A., Laird N., Rubin D., 1977, J. Royal Statist. Society Series B, 39, 1
- Douc R., Guillin A., Marin J.-M., Robert C., 2007, ESAIM: Probability and Statistics, 11, 427
- Dunkley J., Komatsu E., Nolta M. R., Spergel D. N., Larson D., Hinshaw G., Page L., Bennett C. L., Gold B., Jarosik N., Weiland J. L., Halpern M., Hill R. S., Kogut A., Limon M., Meyer S. S., Tucker G. S., Wollack E., Wright E. L., 2009, ApJS, 180, 306
- Efstathiou G., 2008, MNRAS, 388, 1314
- Eisenstein D. J., Zehavi I., Hogg D. W., Scoccamarro R., Blanton M. R., Nichol R. C., Scranton R., Seo H.-J., Tegmark M., Zheng Z., et al., 2005, ApJ, 633, 560
- Feroz F., Hobson M. P., 2008, MNRAS, 384, 449
- Feroz F., Hobson M. P., Bridges M., 2009, MNRAS, 398, 1601
- Heavens A. F., Kitching T. D., Verde L., 2007, MNRAS, 380, 1029
- Hinshaw G., Weiland J. L., Hill R. S., Odegard N., Larson D., et al., 2009, ApJS, 180, 225
- Jeffreys H., 1939, Theory of Probability, first edn. The Clarendon Press, Oxford
- Jeffreys H., 1961, Theory of Probability, third edn. Oxford Classic Texts in the Physical Sciences, Oxford University Press, Oxford
- Komatsu E., Dunkley J., Nolta M. R., Bennett C. L., Gold B., Hinshaw G., Jarosik N., Larson D., Limon M., Page L., Spergel D. N., Halpern M., Hill R. S., Kogut A., Meyer S. S., Tucker G. S., Weiland J. L., Wollack E., Wright E. L., 2009, ApJS, 180, 330
- Kowalski M., Rubin D., Aldering G., Agostinho R. J., Amadon A., Amanullah R., Balland C., Barbary K., et al., 2008, ApJ, 686, 749
- Kullback S., Leibler R. A., 1951, Annals of Mathematical Statistics, 22, 79
- Lepage G. P., 1978, J. Comput. Phys., 27, 192
- Lindley D., 1957, Biometrika, 44, 187
- Liu J., Chen R., 1995, JASA, 90, 567
- MacKay D. J. C., 2002, Information Theory, Inference & Learning Algorithms. Cambridge University Press, Cambridge, UK
- Marin J.-M., Robert C. P., 2010, in Frontiers of Statistical Decision Making and Bayesian Analysis (to appear), Springer-Verlag New York
- Martin J., Ringeval C., 2006, Journal of Cosmology and Astro-Particle Physics, 8, 9
- Ménard B., Kilbinger M., Scranton R., 2009, Submitted to MNRAS, also arXiv:0903.4199
- Mukherjee P., Parkinson D., Liddle A. R., 2006, ApJ, 638, L51
- Parkinson D., Mukherjee P., Liddle A. R., 2006, Phys. Rev. D, 73, 123523
- Peebles P. J. E., 2002, arXiv:astro-ph/0208037
- Peiris H. V., Easther R., 2006, Journal of Cosmology and Astro-Particle Physics, 7, 2
- Robert C. P., Wraith D., 2009, in Proceedings of MaxEnt 2009, to be published by American Institute of Physics, also arXiv:0907.5123
- Schrabback T., Hartlap J., Joachimi B., Kilbinger M., Simon P., et al., 2009, Submitted to A&A, also

- arXiv:0911.0053
Schwarz G., 1978, *Ann. Statist.*, 6, 461
Serra P., Heavens A., Melchiorri A., 2007, *MNRAS*, 379, 169
Skilling J., 2006, *Bayesian Analysis*, 1(4), 833
Trotta R., 2007, *MNRAS*, 378, 72
Trotta R., 2008, *Contemporary Physics*, 49, 71
Vardanyan M., Trotta R., Silk J., 2009, *MNRAS*, 397, 431
Waterhouse T. P., Zibin J. P., 2008, *ArXiv e-prints*
Wraith D., Kilbinger M., Benabed K., Cappé O., Cardoso J.-F., Fort G., Prunet S., Robert C. P., 2009, *Phys. Rev. D*, 80, 023507 (WKB09)